ACS OMEGA

http://pubs.acs.org/journal/acsodf

Article

Electrochemistry as a Complementary Technique for Revealing the Influence of Reducing Agent Concentration on AgNPs

Sapokazi Timakwe, Bongiwe Silwana, and Mangaka C. Matoetoe*

Cite This: *ACS Omega* 2022, 7, 4921−4931

Read Online

ACCESS | Metrics & More | Article Recommendations | Supporting Information

ABSTRACT: The synthesis process of AgNPs has been attracting a lot of attention in the fields of biosensors/sensors, diagnostics, and therapeutic applications. An attempt to understand the effect of different concentrations of reducing agents on the synthetic design process has been made. In this paper, we gather information on voltammetry studies and relate it with UV−vis and scanning electron microscopy (SEM) analyses. Given the kinetics, localized surface plasmon absorption (LSPR) band, and narrow size distribution of these methods, it was possible to compare the obtained measurements and clearly distinguish sizes and aggregation. AgNPs measured by SEM showed a statistically significant reduction of the nanoparticle sizes from 65 to 37.5 nm as the reducing agent increased. Well-matched *d*-spacing data calculated from selected area electron diffraction (SAED) patterns and X-ray diffraction (XRD) were obtained for all of the samples. The UV−vis studies showed that the SPR bands shift toward the blue region as the reducing agent concentration is increased, indicating a decrease in particle sizes. It is worth emphasizing that cyclic voltammetry (CV) and differential pulse voltammetry (DPV) coincide well with SEM on the aggregation of AgNPs at higher concentrations. A 10 mM reducing agent concentration resulted in uniform outcomes for producing AgNPs with the smallest size in terms of full width at half-maximum (FWHM) in all of the methods used in this study, while UV−vis band gaps increase with increasing reducing agent concentration. In agreement with all of the methods investigated, the results suggested that the best concentration of the reducing agents is 10 mM for a target application. These findings suggest the usefulness of voltammetry as a complementary method that can be used as a qualitative guide to identify the size and aggregation of NPs.

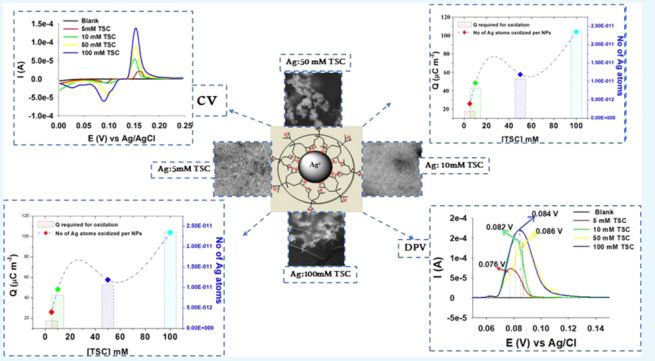

INTRODUCTION

Nanomaterials appear to have a vital role in materials science, chemistry, physics, and medicine, already finding applications in several fields, including therapeutic, diagnostic, and sensors.[1−6] According to research, the preparation of nanoparticles depends on many experimental conditions, including the choice of a reducing agent. Understanding the reasons for the aggregation, shape, surface, and change of size of nanoparticles after integration into a target application is critical for optimizing performance. Among metallic nanoparticles, silver nanoparticles (AgNPs) are the most studied nanomaterials because of their attractive properties such as their versatility in synthesis, easy processability, fast kinetic reaction rate, and high thermal and chemical stability. In addition to this, AgNPs often have general dispersibility and a wide size distribution, which may inevitably generate imprecise results.[7]

Countless procedures have been used for the preparation of AgNPs.[8−10] However, wet chemical reduction process is one of the simplest and advantageous methods with a better yield compared to physical procedures. Wet chemical methods mainly use three main components, which are metal precursors, reducing agents, and stabilizing/capping agents. In most of the synthesis methods, reducing agents are used in excess with regard to stoichiometric quantities. This makes the process complicated. It is important to mention that the current tendency is to find reaction conditions where the reducing agent is also in charge of directing the structure and being a stabilizer of the final product.

Many methods have been used to optimize the synthesis parameters of AgNPs, especially to reduce the size and improve their physicochemical properties.[11,12] However, although there are well-established techniques for the monitoring of experimental factors in the synthesis of nanoparticles, it is necessary to investigate simple electrochemical methods that require short reaction times and low

Received: October 5, 2021
Accepted: November 23, 2021
Published: February 4, 2022

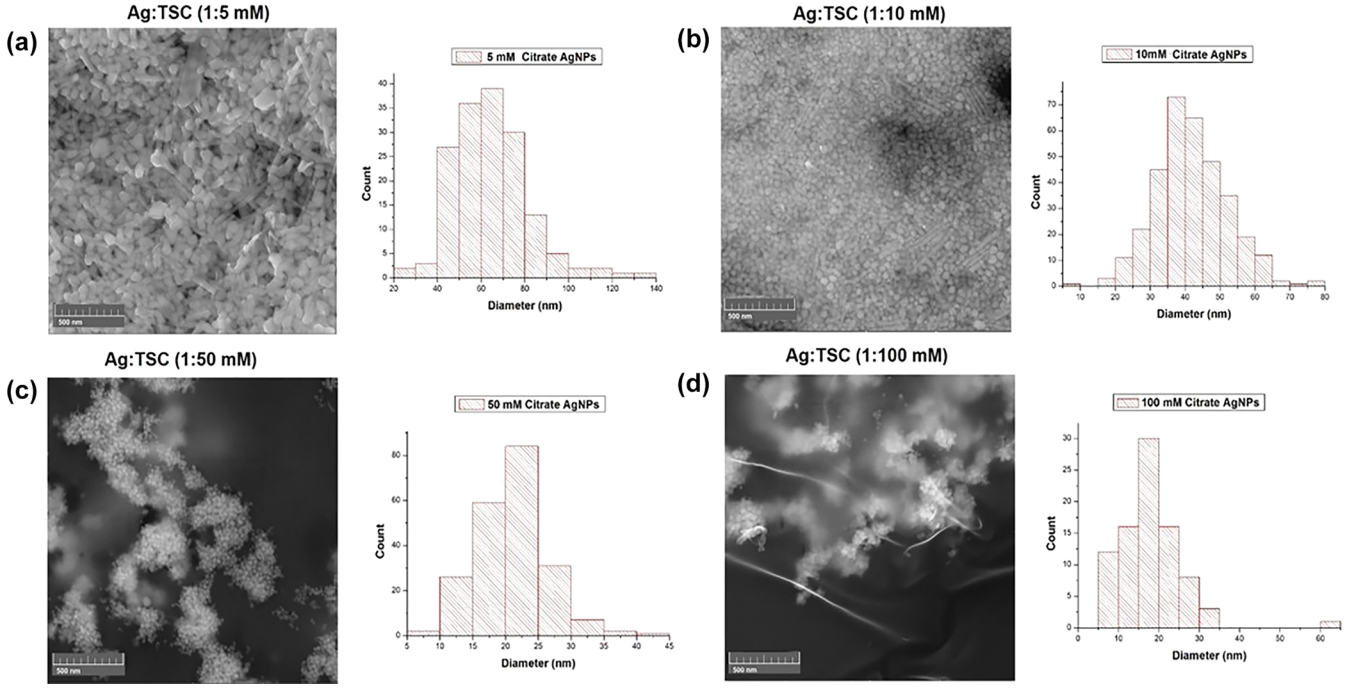

Figure 1. SEM images of AgNPs in Ag/TSC ratios of (a) 1:5, (b) 1:10, (c) 1:50, and (d) 1:100 and the corresponding diameter histograms.

cost. Electrochemical methods offer detailed information on the surface structure of shape-controlled metal nanoparticles based on many nanoparticles that are available on the electrode surface.[13−16] However, scientific research is lacking data on electrochemical methods for investigating the size and aggregation of AgNPs.

Synthesis of Ag nanoparticles in a controlled manner is still difficult because of the lack of design principles that allow accessing the desired structures in a predictive manner. Several reducing agents play a major role in the formation of metal salts into metal nanoparticles, which are important parameter selections in the shape and size of nanoparticles. Also, the potential application of any nanoparticle is strongly dependent on its stability against aggregation. In most cases, the application of AgNPs is to a certain extent limited by the common problem of dispersion instability against aggregation. This process ended up in the formation of large aggregates that decrease the active surface area and therefore result in a significant decrease in their unique properties. This encouraged our group to investigate electrochemical methods for monitoring AgNPs at different reducing agents' concentrations and compare them with other traditional methods. This research method is unique since it has not been conducted on any reducing agent to study different concentrations in order to investigate the size and aggregation. Also, it is the first study to establish electrochemistry and relate it to microscopic and spectroscopic methods. With this point of view, we address the issue of transitions that may occur on the synthesis of Ag nanoparticles and how these methods can be effectively combined and how they can complement each other. One of the most relevant aspects in the production of AgNPs is that their resultant color presents a high dependence on their size and shape.[17]

In this work, trisodium citrate (TSC) was used as a reducing agent in ratios of $AgNO_3$/TSC (1:5); (1:10); (1:50), and (1:100) to observe the effect of its concentration. An experimental setup was investigated to determine optimal synthesis conditions in order to produce small well-dispersed AgNPs of uniform sizes in a simple and cost-effective way by just modulation of the concentration of TSC. The unique optical, electrical, and thermal properties, high electrical conductivity, and biological properties of AgNPs resulted in an increase in their use in various fields, including medical, food, healthcare, consumer, and industrial purposes.[3,18−20] These peculiar properties have been used in many applications, which include antibacterial agents, in industrial, household, and healthcare-related products, consumer products, medical device coatings, optical sensors, cosmetics, pharmaceutical industry, food industry, diagnostics, orthopedics, drug delivery, and as anticancer agents and have ultimately enhanced the tumor-killing effects of anticancer drugs.[21] The latest application of AgNPs is in many textiles, keyboards, wound dressings, and biomedical devices.[22,23] We are also emphasizing the specific applications of AgNPs on constructing electrodes, such as silver coral-like nanostructures on graphite electrodes suitable for bioelectronic applications[24] and pillar-like silver nanostructures on graphite plate electrodes suitable for environmental applications.[25]

Since AgNPs are important in various applications, the optimal synthesis conditions have been obtained. In this work, a comparison of the properties of the synthesized materials at various TSC concentrations using various techniques is detailed. A report on the correlation of these properties studied by optical (UV−vis), electrochemical (CV and DPV), and microscopic (SEM) properties is given. The similarities and differences of each method are discussed, especially with respect to the size and ability to distinguish their degrees of aggregation. While cyclic voltammetry (CV) and differential pulse voltammetry (DPV) are unable to quantify the size, they can give some insights into the size of the nanoparticle. It is well established that a scanning electron microscope is able to give quantitative information on particle sizes. This article shows that it is possible to use voltammetry to get some of the information that is vital and needed on size and aggregation.

https://doi.org/10.1021/acsomega.1c05374
ACS Omega 2022, 7, 4921−4931

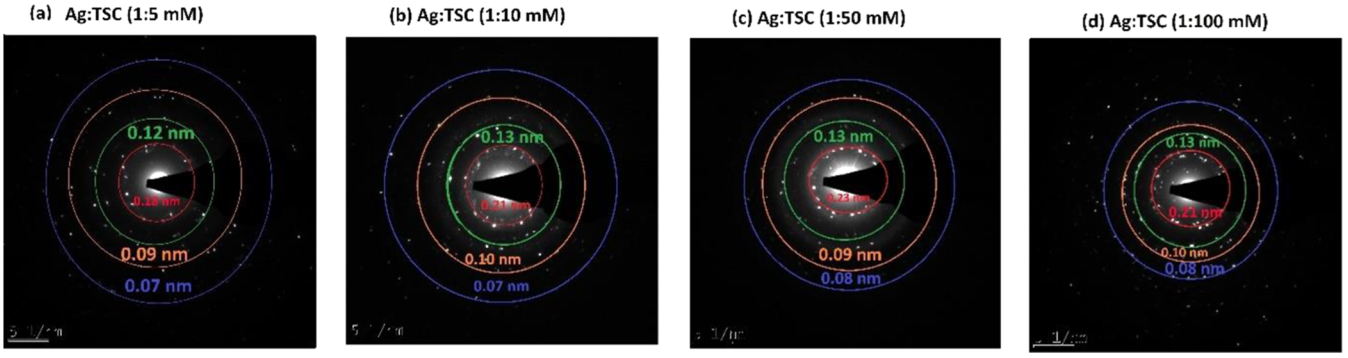

Figure 2. Selected area diffraction patterns of different AgNPs obtained from different Ag/TSC ratios of (a) 1:5, (b) 1:10, (c) 1:50, and (d) 1:100.

RESULTS AND DISCUSSION

Scanning Electron Microscope (SEM). Figure 1 shows SEM images of AgNPs produced by varying the TSC reducing agent concentrations. The size distribution was investigated statistically by measuring the diameter of random nanoparticles.

At lower concentrations of TSC (5 and 10 mM), the SEM images showed a mixture of well-dispersed AgNPs of different shapes (spherical and nanorods) distributed over the entire surface of the sample holder without any substantial aggregation. When concentrations of the citrate reducing agent were 5 and 10 mM, the majority portion of the AgNPs was spherical in shape with estimated average diameters of 65 and 37.5 nm, respectively. Increasing the citrate reducing agent concentration from 50 to 100 mM led to a decrease in particles with an average diameter of 22.5−17.5 nm.

The large variety of particle shapes produced at 5 and 10 mM visualized by SEM is also justified by the broader localized surface plasmon absorption (LSPR) bands of the particles in UV−vis spectra (*vide infra*). At higher concentrations (50 and 100 mM) of the reducing agent, although adding more citrate concentration produced smaller AgNPs, which is an indication of the good sensitivity in comparison to 5 and 10 mM concentrations, some evidence of aggregation was seen; smaller nanoparticles coalesced with each other, leading to bigger NPs, which were less distributed, forming clusters and bunches that did not cover the entire surface of the holder. The reason might be due to a decrease in the interaction of NPs. These aggregates can have an effect on the homogeneity of the film, which is an important issue in the construction of electrochemical sensors and biosensors. SEM statistical analysis also agree with the wavelength and band-gap evaluation results. However, the smaller size range observed in SEM for 50 and 100 mM concentrations is inconsistent with their corresponding full width at half-maximum (FWHM) observed by UV−vis, CV, and DPV, which predicted the narrowest sizes at 10 mM concentration of the reducing agent. Referring to Figure 1, we have concluded that the use of different concentrations of reducing agents leads to different particle sizes, and high concentrations resulted in the aggregation of AgNPs. The sizes are on the order of 5 > 10 > 50 > 100 nm, which is in agreement with UV−vis plasmon bands.

Selected Area Electron Diffraction. The selected area electron diffraction (SAED) images for different concentrations of the reducing agent showed diffused ring structures that are characteristic of polycrystalline Ag, as shown in Figure 2a−d.

All of the SAED patterns of the samples showed a strong bright ring diffraction feature at 0.12−0.23 nm with a strong link to (111) and (220) of Ag planes as seen in Figure 2. The *d*-spacing values by the fast Fourier transform (FFT) image (figure not shown) at 5, 10, 50, and 100 mM concentrations of the reducing agent were calculated to be 0.19,0.23, 0.24, and 0.38 nm, respectively (Table 2). The X-ray diffraction (XRD) exhibited four crystalline planes at (111), (200), (220), and (311) of AgNPs with *d*-spacing values of 0.23, 0.21, 0.14, and 0.12 nm, which agree with studies done by Murthy and coworkers.[26] To obtain further understanding of the *d*-spacing, we compared these values with the ones from X-ray diffraction (XRD) and found that the values we obtained were very close to the XRD pattern. The HR-TEM images of the different concentrations of the reducing agents are presented in Figure S3 of the Supporting Information.

UV−Vis Analysis. Figure 3 shows the UV−vis spectra of AgNPs prepared using various concentrations (10, 20, 50, and

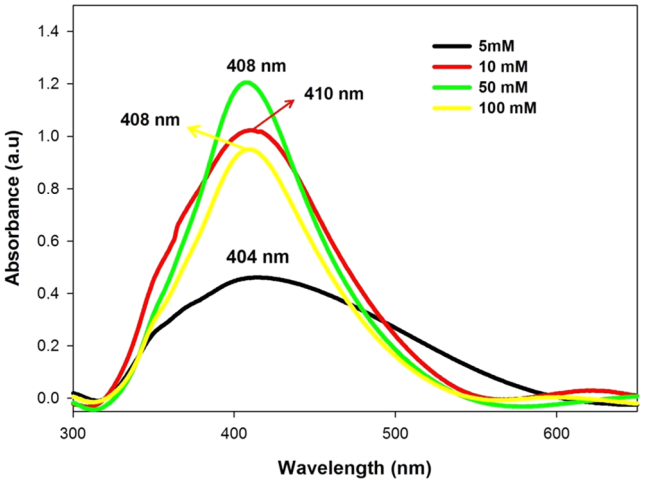

Figure 3. UV−visible spectra of AgNPs obtained with different weight ratios of trisodium citrate.

100 mM) of trisodium citrate. The localized surface plasmon absorption (LSPR) changes of AgNPs are well-known sensitive indicators in nanoparticle formation.

AgNPs exhibited strong LSPR bands of 404, 410, 408, and 408 nm (Figure 3), which are generally related to particle sizes. The 5 and 10 mM concentrations showed single unsymmetrical broad LSPR bands, while 50 and 100 mM concentrations showed only a single symmetrical band, which is an indication of spherical nanoparticles. Mie's theory

https://doi.org/10.1021/acsomega.1c05374
ACS Omega 2022, 7, 4921−4931

Scheme 1. Schematic Illustration Mechanism for the Reaction Progress when Silver Nitrate Precursor Was Used in the Preparation of AgNPs

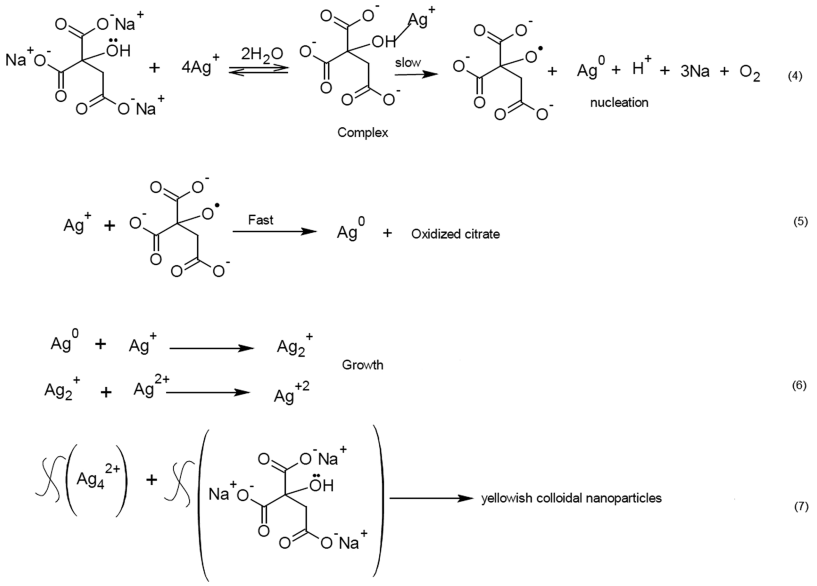

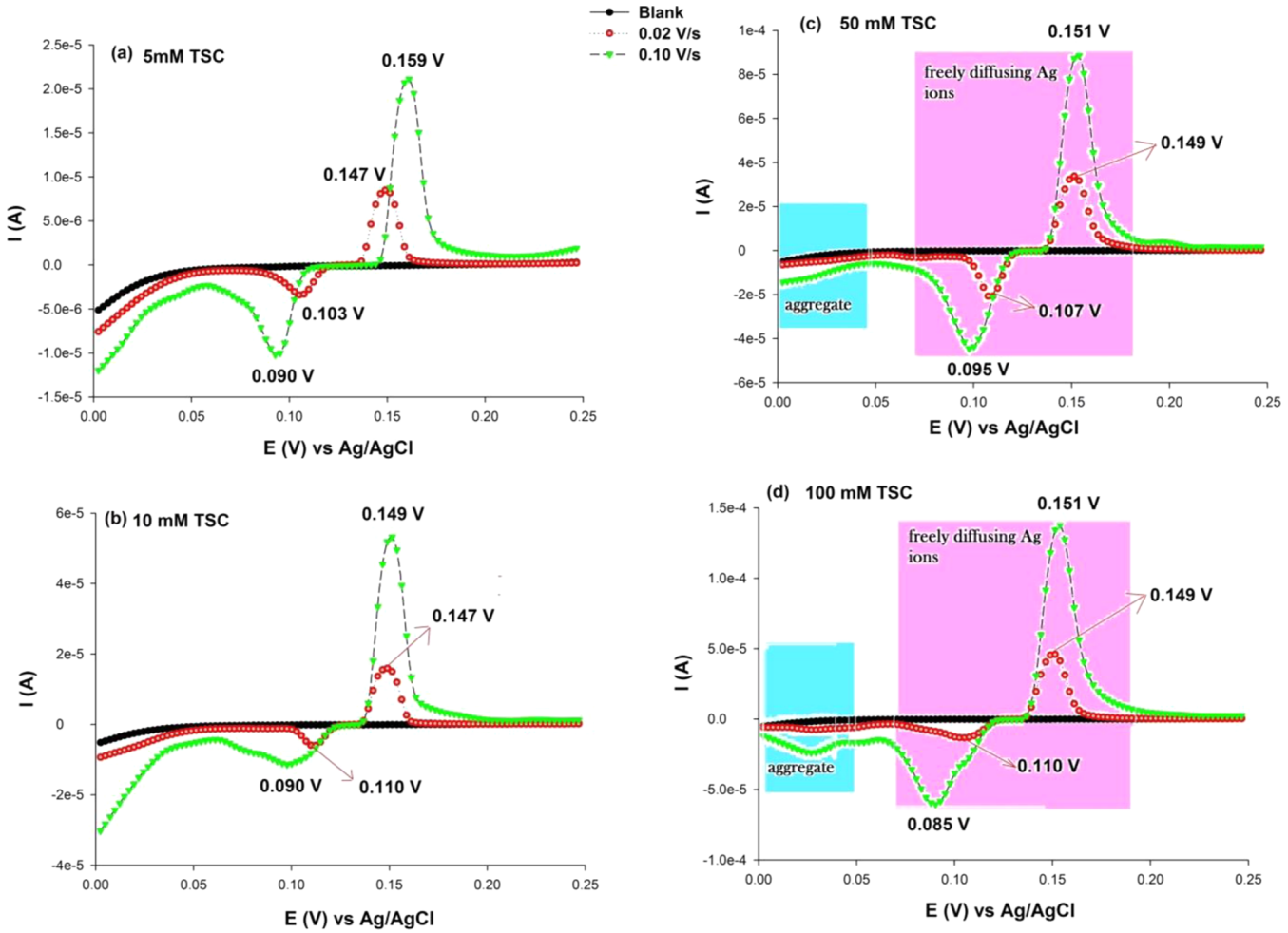

Figure 4. Cyclic voltammograms of AgNP films on GCE. The AgNPs were obtained in different Ag/TSC ratios of (a) 1:5, (b) 1:10, (c) 1:50, and (d) 1:100.

stated that only a single band is expected in the absorption spectra of spherical nanoparticles, which indicates that electrons oscillate, only on one main axis.[27] Smitha and co-workers added that the position of the UV−vis band depends

https://doi.org/10.1021/acsomega.1c05374
ACS Omega 2022, 7, 4921−4931

Table 1. Kinetic and Thermodynamic Parameters of AgNPs Evaluated Based on Oxidation and Reduction Peaks at Different Concentrations of the Reducing Agent

[TSC] mM	ΔE_p (V)	n	De ($cm^2\ s^{-1}$) × 10^{-12}	$K_s\ s^{-1}$	Q $\mu C\ cm^{-2}$ (DPV)	Q $\mu C\ cm^{-2}$ (CV)	ΔG (J·mol)
5	0.069	0.71	8.65	4.5×10^{-3}	10.79	17.67	−4726.81
10	0.059	0.76	9.31	1.6×10^{-2}	20.08	42.56	−4326.40
50	0.056	0.75	9.13	7.8×10^{-3}	30.44	52.84	−4053.07
100	0.066	0.75	9.12	4.5×10^{-3}	36.61	104.44	−4776.02

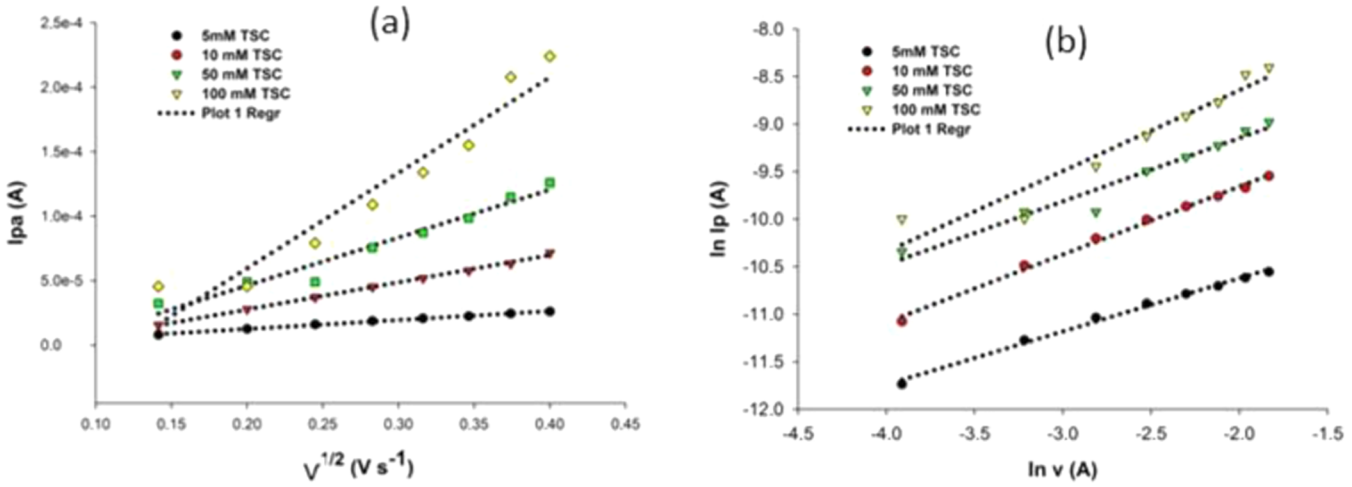

Figure 5. Randle's plots of the anodic peak current against the square root of scan rate (a) and plot of the In peak current against the In scan rate (b) of the AgNP (obtained using different concentrations of TSC) films on a GCE.

on the particle size, shape, composition, state of aggregation, and the surrounding dielectric medium.[28] We have seen the broadening of the SPR bands at 5 and 10 mM concentrations toward longer wavelengths (red shift), which is an indication of nanoparticles with various shapes and sizes.[29] Color changes at various concentrations are also observed, as presented in Figure 9 in the experimental part. In Figure 3, the LSPR band was seen to have blue-shifted from 410 to 408 nm due to a decrease in size by increasing the concentration of the reducing agents, which is in agreement with the SEM statistical analysis.

Electrochemical Behavior of AgNPs/GC. The detailed synthesis and reaction mechanism of AgNPs are shown in Figure 9 and Scheme 1 in the experimental part. CV measurements of AgNP-coated GCE with different concentrations of the reducing agent were recorded, as can be seen in Figure 4.

In this discussion, we will briefly summarize the most important findings of the study to obtain a general picture of the redox behavior and changes in cyclic voltammograms at lower and higher scan rates. Regarding the 5 mM concentration, at the scan rates of 0.02 and 0.1 V/s vs Ag/AgCl, a large shift was observed in both oxidation and reduction peaks, while there was a slight shift at other concentrations, i.e., 10, 50, and 100 mM. It is apparent that the oxidation peaks at all concentrations can be attributed to Ag ions, and the reduction peaks are associated with a reduction of Ag^+ to Ag^0. The system showed a chemically quasi-reversible one-electron redox process with a peak-to-peak separation ΔE_p equal to or very close to 0.059 V (values are listed in Table 1). These observations have been frequently reported in AgNP electrochemical studies.[30−32] Concentrations of 50 and 100 mM of the reducing agent showed a peak that might possibly be related to aggregates, as highlighted in blue in the voltammogram. This was confirmed by varying the scan rate, as shown in Figure S1.

Likewise, SEM results also revealed the aggregates in 50 and 100 mM TSC reducing agent concentrations (Figure 1). Both the anodic and cathodic peaks' current increases with an increasing scan rate, indicating the kinetic effects, as illustrated in Figures S1 and S2. The oxidation and reduction peaks' potential between scan rates 0.04 and 0.16 tends to be stable with a 5 mM reducing agent. The oxidation peaks remain stable between 0.04 and 0.16 V/s for 10, 50, and 100 mM, while the reduction peak at a higher scan rate tends toward a less positive voltage potential. The plot of I_{pa} vs square root of the scan rate (Figure 5a) was linear for concentrations 5, 10, and 50 mM, while there was a lack of linearity in the plot of I_p vs square root of the scan rate at a concentration of 100 mM reducing agent. Generally, the current (I_{pa}) is proportional to the square of the scan rate, where charge transfer is the diffusion limit. All of the systems show linear diffusion conditions. The Randles−Sevcik relation for the one-electron reaction can be applied, and the apparent diffusion coefficient was deduced using the Randles−Sevcik relation.[33]

$$I_p = 2.69 \times 10^5\, n^{2/3} \cdot A \cdot D_{OX}^{1/2} \cdot C_{OX}^{*} \cdot V^{1/2} \quad (1)$$

where I_p is the peak current, V is the scan rate (V/s), A is the electrode area (cm^2), n is the number of electrons transferred, and D is the diffusion coefficient. The values obtained are tabulated in Table 1, which show the bigger value at the 10 mM reducing agent concentration. According to the Stokes−Einstein equation, the smaller molecule should have a higher diffusion coefficient (De) than the comparatively larger molecule, so AgNPs prepared by the 10 mM reducing agent are the smallest since they gave a high value of De, as listed in Table 1.[34,35]

https://doi.org/10.1021/acsomega.1c05374
ACS Omega 2022, 7, 4921−4931

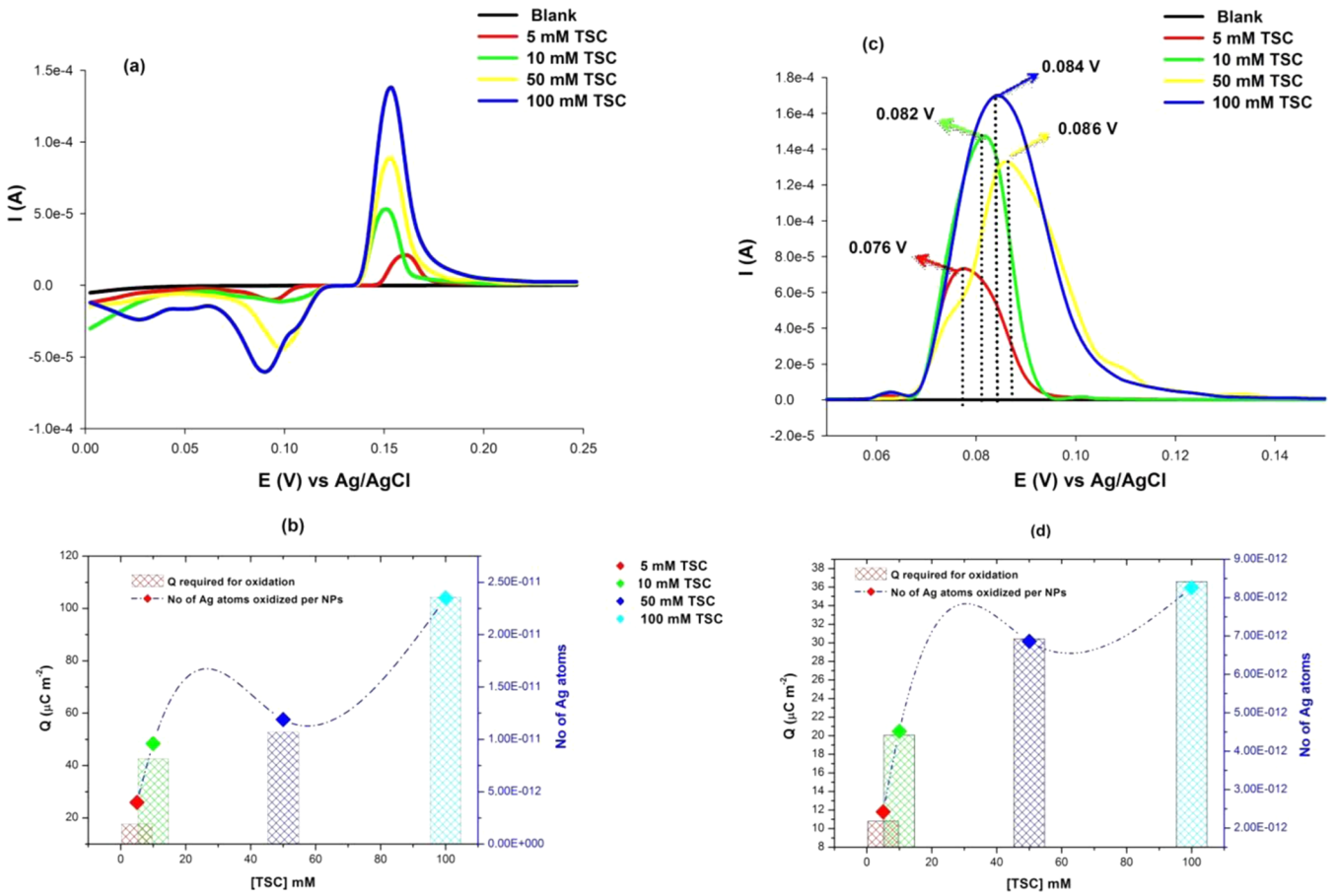

Figure 6. Overlay of cyclic (a) and differential pulse (c) voltammograms measured in a 0.1 M HCl solution: (b, d) charge and number of Ag atoms versus the concentration of trisodium citrate (TSC). CV parameters: scan rate 0.1 V/s. DPV parameters: potential step 8 mV, pulse width 40 ms (5 ms of waiting time and 20 ms for current sampling time), pulse amplitude 50 mV, without an accumulation step.

$$K_s = \frac{I_p}{n\mathrm{FAC}} \quad (2)$$

Heterogeneous rate constant (K_s) is an important diagnostic criterion for predicting the nature of a redox process. To identify the size of AgNPs, these values will be of importance in this study as we know that large NPs will travel the most slowly in solution due to the mass and result in small values of K_s. In contrast, small NPs will be quick and result in large K_s values. The value of the rate constant at 10 mM was found to be the largest, indicating smaller AgNPs. The calculated values also fall in the range of a quasi-reversible redox system, supporting our attribution of a quasi-reversible system. The negative values of Gibbs free energy reveal the spontaneity of the redox process (Table 1). Brainina and co-workers assumed that the change in Gibbs free energy of the NPs is associated with a decreasing size (Plieth's theory), which leads to a negative shift in E_p.[36−38] Our experimental ΔG does not follow the theoretical trend. The reasons behind this discrepancy are not clear at this moment.

The slope value of ln I_p vs ln scan rate is 0.560 for the 5 mM concentration, which is very close to 0.5, thus indicating the redox process to be limited by diffusion, while the values for 10, 50, and 100 mM concentrations are 0.715, 0.667, and 0.850, respectively. This is an indication of a mixture of adsorption and diffusion controlled system. According to the literature, as the nanoparticle sizes decrease, peak potentials move to more negative potentials. Figure 6 shows the oxidation potentials of CV and DPV in comparison to the behavior of different concentrations of the reducing agent (TSC). Based on oxidation potentials, we were able to determine the size of the nanoparticles or determine if aggregation has occurred.

Theoretical and most of the experimental studies have proven that as the radius of metal nanoparticles decreases, so does their oxidation potential. Plieth similarly predicted that the smaller the size of NPs, the more the negative shift in oxidation potentials due to the greater exposed surface area compared to larger ones.[38] Considering all of these predictions, we have scrutinized the CV and DPV oxidation potentials comparing the concentrations of the studied reducing agent. The concentration of TSC affected the recorded redox peak current, as can been seen by a shift in peaks in CV, especially at 5 and 10 mM concentrations (Figure 6a). Stable and prominent oxidation signals were observed in CV at TSC concentrations of 50−100 mM, and their reduction products shifted cathodically. However, a quite different situation from DPV was encountered when the positive shift appeared in all of the concentrations of the reducing agent. This might be due to aggregation when small NP aggregates tend to oxidize at potentials corresponding to larger nanoparticles. AgNPs prepared by 50 and 100 mM reducing agent concentrations exhibited a greater decrease in the surface area from small isolated nanoparticles to bigger aggregates and exhibited a positive shift in the oxidation potential. At 50 mM TSC, a prominent signal was observed, unlike in CV, where it was

https://doi.org/10.1021/acsomega.1c05374
ACS Omega 2022, 7, 4921−4931

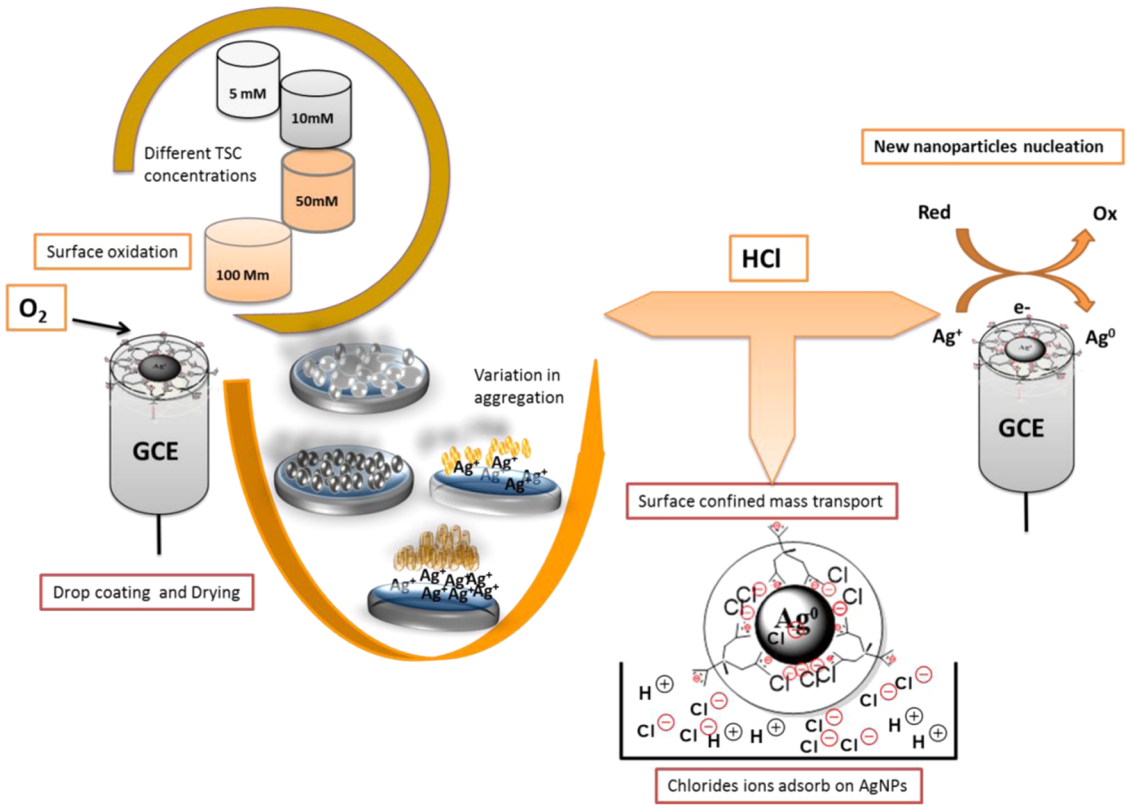

Figure 7. Proposed pathway for new nanoparticle formation from parent AgNPs on a GCE.

observed at 100 mM. The charge released reflects the extent of the surface oxidation, thus revealing the extent to which internal surfaces are electroactive. A nonlinear correlation on the variations of the number of atoms oxidized and the histogram of the charge passed (Q/C) as a function of TSC concentrations for the oxidation process of AgNPs is shown in Figure 6b,d. Remarkably, both charge and the number of Ag atoms that are oxidized increase as the reducing agent concentration increases in CV and DPV.

Transformation of AgNPs in Chloride Anions on a GCE. An illustration of the possible mechanism involved in the transformation of AgNPs in chloride anions is given in Figure 7. Electrochemical measurements revealed aggregation in 50 and 100 mM reducing agents as evidenced by SEM analysis. To elucidate the mechanism of these different concentrations on the surface of GCE in HCl as an electrolyte solution, we propose the following mechanism.

Based on the information we obtained in the voltammetry measurement, the presence of higher concentrations (50 and 100 mM) of the reducing agent was seen to form aggregates with large AgNP sizes compared to the information we obtained from their diameters, LSPR bands, and band gaps. Piella and co-workers once mentioned in their study that aggregation processes rarely occur alone and always simultaneously take place with oxidation and dissolution.[39−41] We speculate that the drying process and the electrolyte solution might have an influence on changes experienced in these experimental outcomes. We proposed the first scenario of aggregation that occurred under oxygenated conditions during the drying process; AgNPs lead to the liberation of Ag^+ ions, as can be seen in Figure 7. We postulated that Ag−citrate bonds lose stability and the NPs interact with each other to form aggregates. The second scenario was introducing HCl as an electrolyte solution; this might also be responsible for the formation of aggregates and the AgCl layer according to the following reaction

$$4Ag^+ + 4Cl^- + O_2 \rightarrow 2AgCl + 4OH^- \quad (3)$$

$$AgCl + e \rightarrow AgNPs + Cl^- \quad (4)$$

According to the mechanism, HCl ions displace citrate from the surface, thus disrupting the charge layer of the AgNPs and allowing the AgNPs to aggregate. When Ag^+ ions that are released to the bulk and Cl^- ions interact, AgCl spontaneously forms, which accelerates the oxidation of Ag. By observing the charge values that increased with the reducing agent concentration thus suggesting that in 50 and 100 mM NPs films on GCE there are more silver atoms exposed to HCl solution, but only NPs that are oxidized into Ag^+ are the ones that are in contact with the electrode. As the Ag^+ ions dissolve in the electrolyte solution, the rest of the aggregated NPs lose electrical contact with the electrode, and the remaining NPs inside the aggregates are not oxidized. The direction of the scan is reversed to promote the reduction of AgCl to obtain new AgNPs.

In addition to the spectra and voltammograms, the full width at half-maximum (FWHM) was plotted in correlation to the SEM particle size response to the reducing agent concentration. In the graph in Figure 8, the particle sizes are displayed in black. Generally, larger molecules would result in a bigger red shift and a broader FWHM. It is evident that in all of the methods used in this study, FWHM follows the same trend with the exception of CV results at 100 mM. With the exception of 100 mM in CV, there was a correlation in all of these results. Notable in all of these methods, the 10 mM reducing agent showed the minimum value of FWHM,

https://doi.org/10.1021/acsomega.1c05374
ACS Omega 2022, 7, 4921−4931

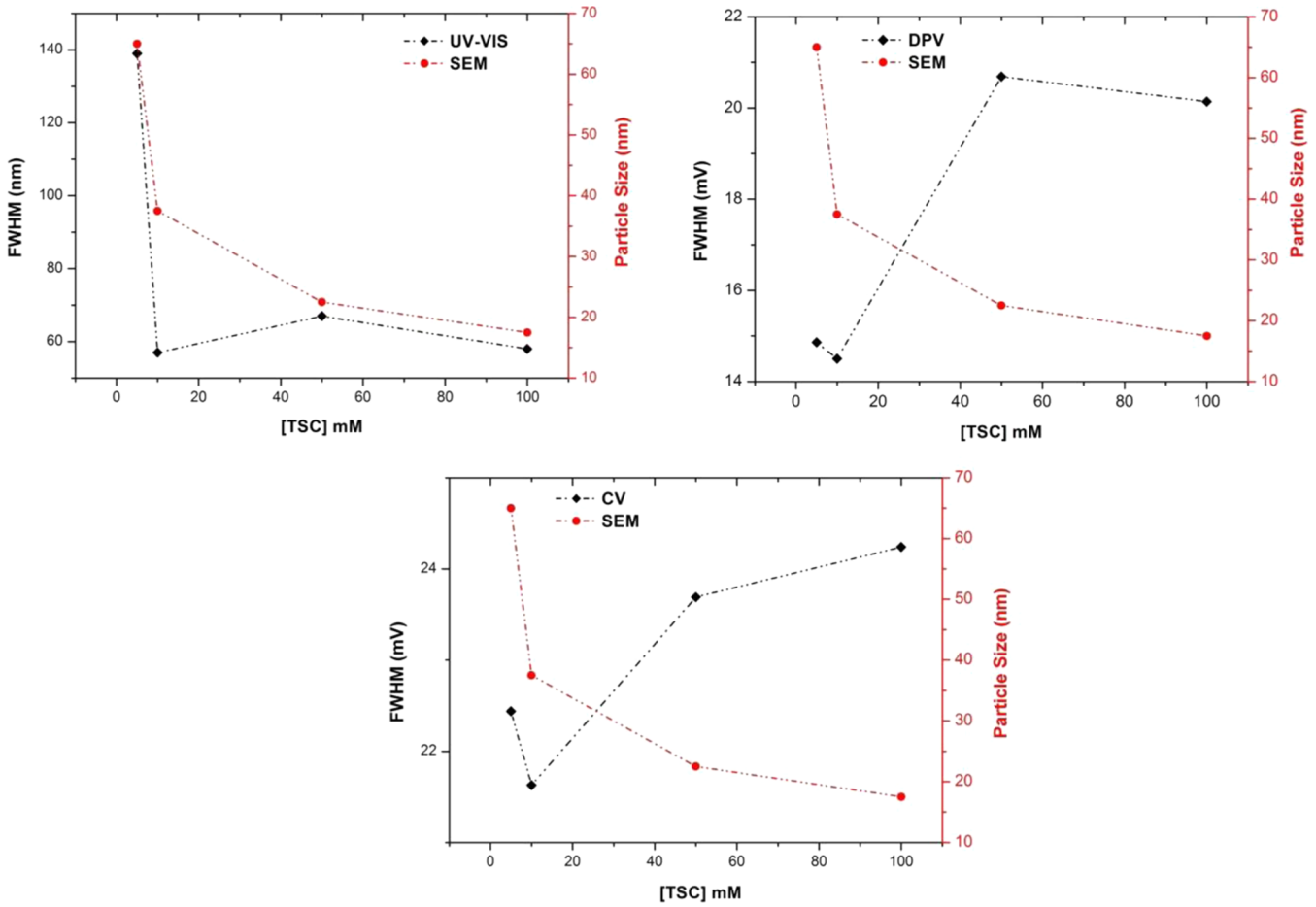

Figure 8. Full width at half-maximum (FWHM) and particle sizes as a function of the reducing agent concentration.

Table 2. Experimental Particle Sizes of AgNPs Analyzed by Electrochemical Methods and UV−Vis Spectra of Different Concentrations of TSC (n = 3)

Ag/TSC Molar ratio	λ (nm)	band gap (eV)	FWHM (UV−vis) (nm)	FWHM (DPV) (mV)	FWHM (CV) (mV)	d-spacing (nm)	particle size (SEM) (nm)
1:5	415	2.99	139	14.9	22.4	0.19	65.0 ± 0.75
1:10	410	3.03	57	14.5	21.6	0.23	37.5 ± 0.56
1:50	408	3.04	67	20.7	23.7	0.24	22.5 ± 1.85
1:100	408	3.04	58	20.1	24.2	0.38	17.5 ± 2.12

indicating the narrowest size distribution. By analyzing the FWHM of the UV−vis spectra, the values show polydispersity and have a large size distribution. The size dependence of the band gap is the most recognizable aspect of quantum confinement.[42] In semiconductors, the band gap increases as the size of the particles decreases.[42,43] Band gaps also increased with increasing reducing agent concentrations. This increase in the band gaps may be due to a decrease in the size of the nanoparticles, which is expected since the surface-to-volume ratio increases for smaller particle sizes. Based on these results, we conclude that different concentrations of the reducing agent strongly affect the particle sizes; high concentrations result in smaller nanoparticles, which aggregate to form clusters and bunches at a later stage, while small concentrations produce larger nanoparticles. We confirmed that small nanoparticles are sensitive toward aggregation of the reducing agent, strongly affecting the particle sizes (Table 2).

CONCLUSIONS

For routine and reliable use of AgNPs for therapeutic and sensor applications, we carried out a study on the effect of varying reducing agent concentrations on nanoparticle synthesis. We used CV and DPV in comparison to UV−visible spectroscopy to measure the width of the peaks of the NPs to extract information on the size and aggregation of the NPs and corroborated these results with SEM. This study provides a useful guideline that will help researchers consider including electrochemistry as a complementary technique when monitoring nanoparticles. We found a dominant role of the TSC concentration on the size and aggregation of AgNPs at concentrations of 50 and 100 mM, and most importantly, the CV and DP also proved the aggregation at the same concentrations. A correlation was found in the FWHM of all of the methods. A concentration of 10 mM gave an FWHM with the narrowest particle size distribution, which indicates the good concentration in comparison to other concentrations. The results indicate the mixture of various shapes and larger

https://doi.org/10.1021/acsomega.1c05374
ACS Omega 2022, 7, 4921−4931

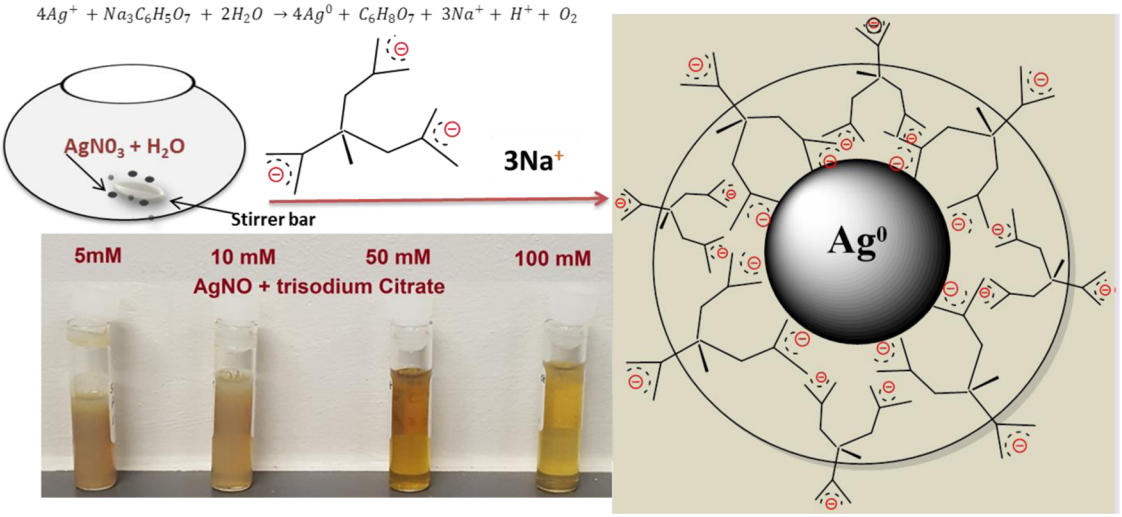

Figure 9. Citrate-capped AgNP formation by the wet chemical method from the chemical reduction of $AgNO_3$ using different concentrations of the reducing agent trisodium citrate and changes in color during the formation of AgNPs.

sizes of the synthesized AgNPs at lower concentrations, while higher concentrations produced small aggregated spherical-shaped NPs. The shape of bands at 5 and 10 mM concentrations evidences the various shapes of NPs. To date, the only indicative evidence in the UV−vis spectra of AgNP aggregation is a decrease in intensity at 100 mM. On the other hand, CV and DPV methods were able to uncover details about aggregation at both 50 and 100 mM concentrations, in agreement with SEM. This proves that voltammetry is more sensitive for identifying aggregates than the UV−vis method. Also, a combination of these methods with careful interpretation of the data is usually the best option. These findings also revealed the contribution of a higher concentration of reducing agents in size and aggregation of NPs and encourage using electrochemistry as a complementary tool to other techniques for identification of NPs.

EXPERIMENTAL SECTION

Reagents and Apparatus. All chemicals were of analytical grade and were used without further purification. Silver nitrate ($AgNO_3$), trisodium citrate ($Na_3C_6H_5O_7$), ethanol, and hydrochloric acid (HCl) were purchased from Sigma. Solutions were prepared using deionized water. The optical properties of nanoparticles were investigated using a double-beam UV−visible 1800-Shimadzu spectrophotometer, Advanced African Technology (Scientific division) serial number 127471. The size distribution and morphology were analyzed using a SEM. SEM images were then analyzed by Image J, a java-based image processing program. Electrochemical measurements were run using a typical conventional one-compartment three-electrode system connected to the potentiostat Autolab PGSTAT 101 (Metrohm, SA) operating in software NOVA 2.1. The three-electrode cell setup consists of GCE, a platinum wire, and a Ag/AgCl electrode. The GCE was polished with 0.05, 0.3, and 1 μM alumina powder to remove any residue deposits on the surface. As part of the daily polishing routine, the GCE was sonicated in water and ethanol for 5 min in between polishing steps. Unless stated otherwise, all experiments were run using 0.1 M HCl solution over the potential range −0.5 to +0.5 V.

Synthesis and Reaction Mechanism of AgNPs. The chemical reduction of $AgNO_3$ in the presence of trisodium citrate (TSC) reducing agent has been outlined previously.[19,44,45] The first approach was using an aqueous solution method in which trisodium citrate was added to a solution of $AgNO_3$ and the mixture was gently stirred overnight at room temperature to reduce the Ag^+ to Ag^o, as can be seen in Figure 9.

Specifically, AgNPs have grown from $AgNO_3$ in the presence of different concentrations of TSC as a reducing agent, keeping the concentration of Ag^+ ions fixed. The addition of trisodium citrate to $AgNO_3$ resulted in an almost instantaneous change of colors, as seen in Figure 9, indicating the effectiveness of the Ag^+ reduction. The AgNPs were collected using an ultracentrifuge for 30 min (8000 rpm), cleaned multiple times, and then analyzed using SEM, optical, and electrochemical methods. The detailed proposed mechanism for the reduction of Ag^+ to Ag^o in this work is explored in Scheme 1. The proposed mechanism implied that the presence of van der Waals forces between the positive charge of Ag+ and the oxygen of the TSC increases the reducing and stabilizing efficiency of TSC on the surface of the AgNPs.

ASSOCIATED CONTENT

Supporting Information

The Supporting Information is available free of charge at https://pubs.acs.org/doi/10.1021/acsomega.1c05374.

Scan rate studies of silver nanoparticles prepared with different concentrations of trisodium citrate characterized by cyclic voltammetry, Randell's plot of anodic peak current vs scan rate of different concentrations of the reducing agent, X-ray diffraction patterns of AgNPs prepared using different concentrations of the TSC reducing agent, and HR-TEM images showing different sizes of AgNPs (PDF)

AUTHOR INFORMATION

Corresponding Author

Mangaka C. Matoetoe − *Department of Chemistry, Cape Peninsula University of Technology, Cape Town 8000, South*

https://doi.org/10.1021/acsomega.1c05374
ACS Omega 2022, 7, 4921−4931

Africa; orcid.org/0000-0002-2662-3535;
Email: lellangm@gmail.com

Authors

Sapokazi Timakwe − *Department of Chemistry, Cape Peninsula University of Technology, Cape Town 8000, South Africa*

Bongiwe Silwana − *Department of Chemistry, Cape Peninsula University of Technology, Cape Town 8000, South Africa*

Complete contact information is available at:
https://pubs.acs.org/10.1021/acsomega.1c05374

Notes

The authors declare no competing financial interest.

■ ACKNOWLEDGMENTS

The authors acknowledge the assistance of the NRF grant (116237) and CPUT in carrying out the study. The authors involved declare that there is no conflict of interest with any institution on this publication.

■ REFERENCES

(1) Astanina, K.; Simon, Y.; Cavelius, C.; Petry, S.; Kraegeloh, A.; Kiemer, A. K. Superparamagnetic Iron Oxide Nanoparticles Impair Endothelial Integrity and Inhibit Nitric Oxide Production. *Acta Biomater.* **2014**, *10*, 4896−4911.

(2) Jha, D. K.; Shameem, M.; Patel, A. B.; Kostka, A.; Schneider, P.; Erbe, A.; Deb, P. Simple Synthesis of Superparamagnetic Magnetite Nanoparticles as Highly Efficient Contrast Agent. *Mater. Lett.* **2013**, *95*, 186−189.

(3) Zhang, X.-F.; Liu, Z.-G.; Shen, W.; Gurunathan, S. Silver Nanoparticles: Synthesis, Characterization, Properties, Applications, and Therapeutic Approaches. *Int. J. Mol. Sci.* **2016**, *17*, No. 1534.

(4) Fathima, J. B.; Pugazhendhi, A.; Venis, R. Synthesis and Characterization of ZrO2 Nanoparticles-Antimicrobial Activity and Their Prospective Role in Dental Care. *Microb. Pathog.* **2017**, *110*, 245−251.

(5) El-Faham, A.; Al-Rasheed, H. H.; Sholkamy, E. N.; Osman, S. M.; Alothman, Z. A. Simple Approaches for the Synthesis of AgNPs in Solution and Solid Phase Using Modified Methoxypolyethylene Glycol and Evaluation of Their Antimicrobial Activity. *Int. J. Nanomed.* **2020**, *15*, 2353−2362.

(6) Sim, W.; Barnard, R. T.; Blaskovich, M. A. T.; Ziora, Z. M. Antimicrobial Silver in Medicinal and Consumer Applications: A Patent Review of the Past Decade (2007−2017). *Antibiotics* **2018**, *7*, No. 93.

(7) Wang, M.; Li, H.; Li, Y.; Mo, F.; Li, Z.; Chai, R.; Wang, H. Dispersibility and Size Control of Silver Nanoparticles with Anti-Algal Potential Based on Coupling Effects of Polyvinylpyrrolidone and Sodium Tripolyphosphate. *Nanomaterials* **2020**, *10*, No. 1042.

(8) Yin, H.; Yamamoto, T.; Wada, Y.; Yanagida, S. Large-Scale and Size-Controlled Synthesis of Silver Nanoparticles under Microwave Irradiation. *Mater. Chem. Phys.* **2004**, *83*, 66−70.

(9) Tang, Y.; Wu, T.; Hu, B.; Yang, Q.; Liu, L.; Yu, B.; Ding, Y.; Ye, S. Synthesis of Thermo- and PH-Responsive Ag Nanoparticle-Embedded Hybrid Microgels and Their Catalytic Activity in Methylene Blue Reduction. *Mater. Chem. Phys.* **2015**, *149−150*, 460−466.

(10) Kim, J. S.; Kuk, E.; Yu, K. N.; Kim, J. H.; Park, S. J.; Lee, H. J.; Kim, S. H.; Park, Y. K.; Park, Y. H.; Hwang, C. Y.; Kim, Y. K.; Lee, Y. S.; Jeong, D. H.; Cho, M. H. Antimicrobial Effects of Silver Nanoparticles. *Nanomedicine Nanotechnology, Biol. Med.* **2007**, *3*, 95−101.

(11) Hasnain, M. S.; Javed, M. N.; Alam, M. S.; Rishishwar, P.; Rishishwar, S.; Ali, S.; Nayak, A. K.; Beg, S. Purple Heart Plant Leaves Extract-Mediated Silver Nanoparticle Synthesis: Optimization by Box-Behnken Design. *Mater. Sci. Eng., C* **2019**, *99*, 1105−1114.

(12) Núñez, R. N.; Veglia, A. V.; Pacioni, N. L. Improving Reproducibility between Batches of Silver Nanoparticles Using an Experimental Design Approach. *Microchem. J.* **2018**, *141*, 110−117.

(13) García-Cruz, L.; Montiel, V.; Solla-Gullón, J. Shape-Controlled Metal Nanoparticles for Electrocatalytic Applications. *Phys. Sci. Rev.* **2019**, *4*, 1−34.

(14) Devivaraprasad, R.; Nalajala, N.; Bera, B.; Neergat, M. Electrocatalysis of Oxygen Reduction Reaction on Shape-Controlled Pt and Pd Nanoparticles—Importance of Surface Cleanliness and Reconstruction. *Front. Chem.* **2019**, *7*, No. 648.

(15) Waters, J. The Concentration of Soluble Extracellular Amyloid-β Protein in Acute Brain Slices from CRND8 Mice. *PLoS One* **2010**, *5*, No. e15709.

(16) Montiel, M. A.; Vidal-Iglesias, F. J.; Montiel, V.; Solla-Gullón, J. Electrocatalysis on Shape-Controlled Metal Nanoparticles: Progress in Surface Cleaning Methodologies. *Curr. Opin. Electrochem.* **2017**, *1*, 34−39.

(17) Rivero, P. J.; Goicoechea, J.; Urrutia, A.; Arregui, F. J. Effect of Both Protective and Reducing Agents in the Synthesis of Multicolor Silver Nanoparticles. *Nanoscale Res. Lett.* **2013**, *8*, No. 101.

(18) Gurunathan, S.; Park, J. H.; Han, J. W.; Kim, J. H. Comparative Assessment of the Apoptotic Potential of Silver Nanoparticles Synthesized by Bacillus Tequilensis and Calocybe Indica in MDA-MB-231 Human Breast Cancer Cells: Targeting P53 for Anticancer Therapy. *Int. J. Nanomed.* **2015**, *10*, 4203−4223.

(19) Li, W.-R.; Xie, X.-B.; Shi, Q.-S.; Zeng, H.-Y.; Ou-Yang, Y.-S.; Chen, Y.-B. Antibacterial Activity and Mechanism of Silver Nanoparticles on *Escherichia Coli*. *Appl. Microbiol. Biotechnol.* **2010**, *85*, 1115−1122.

(20) Mukherjee, P.; Ahmad, A.; Mandal, D.; Senapati, S.; Sainkar, S. R.; Khan, M. I.; Parishcha, R.; Ajaykumar, P. V.; Alam, M.; Kumar, R.; Sastry, M. Fungus-Mediated Synthesis of Silver Nanoparticles and Their Immobilization in the Mycelial Matrix: A Novel Biological Approach to Nanoparticle Synthesis. *Nano Lett.* **2001**, *1*, 515−519.

(21) Chernousova, S.; Epple, M. Silver as Antibacterial Agent: Ion, Nanoparticle, and Metal. *Angew. Chem., Int. Ed.* **2013**, *52*, 1636−1653.

(22) Sondi, I.; Salopek-Sondi, B. Silver Nanoparticles as Antimicrobial Agent: A Case Study on E. coli as a Model for Gram-Negative Bacteria. *J. Colloid Interface Sci.* **2004**, *275*, 177−182.

(23) Li, C.; Zhang, Y.; Wang, M.; Zhang, Y.; Chen, G.; Li, L.; Wu, D.; Wang, Q. In Vivo Real-Time Visualization of Tissue Blood Flow and Angiogenesis Using Ag2S Quantum Dots in the NIR-II Window. *Biomaterials* **2014**, *35*, 393−400.

(24) Feng, J. J.; Hildebrandt, P.; Murgida, D. H. Silver Nanocoral Structures on Electrodes: A Suitable Platform for Protein-Based Bioelectronic Devices. *Langmuir* **2008**, *24*, 1583−1586.

(25) Feng, J. J.; Lu, Y. H.; Gernert, U.; Hildebrandt, P.; Murgida, D. H. Electrosynthesis of SER-Active Silver Nanopillar Electrode Arrays. *J. Phys. Chem. C* **2010**, *114*, 7280−7284.

(26) Ananda Murthy, H. C.; Desalegn Zeleke, T.; Ravikumar, C. R.; Anil Kumar, M. R.; Nagaswarupa, H. P. Electrochemical Properties of Biogenic Silver Nanoparticles Synthesized Using *Hagenia Abyssinica* (Brace) JF. Gmel. Medicinal Plant Leaf Extract. *Mater. Res. Express* **2020**, *7*, No. 055016.

(27) Acharya, D.; Mohanta, B.; Deb, S.; Sen, A. K. Theoretical Prediction of Absorbance Spectra Considering the Particle Size Distribution Using Mie Theory and Their Comparison with the Experimental UV−Vis Spectra of Synthesized Nanoparticles. *Spectrosc. Lett.* **2018**, *51*, 139−143.

(28) Smitha, S. L.; Nissamudeen, K. M.; Philip, D.; Gopchandran, K. G. Studies on Surface Plasmon Resonance and Photoluminescence of Silver Nanoparticles. *Spectrochim. Acta, Part A* **2008**, *71*, 186−190.

(29) Sohrabnezhad, S.; Pourahmad, A.; Mehdipour Moghaddam, M. J.; Sadeghi, A. Study of Antibacterial Activity of Ag and Ag2CO3 Nanoparticles Stabilized over Montmorillonite. *Spectrochim. Acta, Part A* **2015**, *136*, 1728−1733.

(30) Okumu, F. O.; Silwana, B.; Matoetoe, M. C. Application of MWCNT/Ag-Pt Nanocomposite Modified GCE for the Detection of

Nevirapine in Pharmaceutical Formulation and Biological Samples. *Electroanalysis* **2020**, *32*, 3000−3008.
(31) Van der Horst, C.; Silwana, B.; Iwuoha, E.; Somerset, V. Synthesis and Characterization of Bismuth-Silver Nanoparticles for Electrochemical Sensor Applications. *Anal. Lett.* **2015**, *48*, 1311−1332.
(32) Choi, Y.-J.; Luo, T.-J. M. Electrochemical Properties of Silver Nanoparticle Doped Aminosilica Nanocomposite. *Int. J. Electrochem.* **2011**, *2011*, No. 404937.
(33) Bard, A. J.; Faulkner, L. R.; Swain, E.; Robey, C. *Electrochemical Methods: Fundamental and Application*; 2nd ed.; John Wiley & son Inc.: New York, 2001.
(34) Munir, S.; Shah, A.; Zafar, F.; Badshah, A.; Wang, X.; Rehman, Z.; Hussain, H.; Lunsford, S. K. Redox Behavior of a Derivative of Vitamin K at a Glassy Carbon Electrode. *J. Electrochem. Soc.* **2012**, *159*, G112−G116.
(35) Nosheen, E.; Shah, A.; Badshah, A.; Zia-Ur-Rehman; Hussain, H.; Qureshi, R.; Ali, S.; Siddiq, M.; Khan, A. M. Electrochemical Oxidation of Hydantoins at Glassy Carbon Electrode. *Electrochim. Acta* **2012**, *80*, 108−117.
(36) Allen, S. L. Use of Anodic Stripping Voltammetry to Study the Size-Selective Electrophoretic Deposition and Aggregation-Dependent Oxidation of Metal Nanoparticles. Electronic Theses and Dissertations, Paper 3141, 2019.
(37) Toh, H. S.; Batchelor-McAuley, C.; Tschulik, K.; Uhlemann, M.; Crossley, A.; Compton, R. G. The Anodic Stripping Voltammetry of Nanoparticles: Electrochemical Evidence for the Surface Agglomeration of Silver Nanoparticles. *Nanoscale* **2013**, *5*, 4884−4893.
(38) Plieth, W. J. Electrochemical Properties of Small Clusters of Metal Atoms and Their Role in Surface Enhanced Raman Scattering. *J. Phys. Chem. A.* **1982**, *86*, 3166−3170.
(39) Piella, J.; Bastús, N. G.; Puntes, V. Modeling the Optical Responses of Noble Metal Nanoparticles Subjected to Physicochemical Transformations in Physiological Environments: Aggregation, Dissolution and Oxidation. *Z. Phys. Chem.* **2017**, *231*, 33−50.
(40) Li, X.; Lenhart, J. J.; Walker, H. W. Aggregation Kinetics and Dissolution of Coated Silver Nanoparticles. *Langmuir* **2012**, *28*, 1095−1104.
(41) Li, X.; Lenhart, J. J.; Walker, H. W. Dissolution-Accompanied Aggregation Kinetics of Silver Nanoparticles. *Langmuir* **2010**, *26*, 16690−16698.
(42) Movlarooy, T. Study of Quantum Confinement Effects in ZnO Nanostructures. *Mater. Res. Express* **2018**, *5*, No. 035032.
(43) Edvinsson, T. Optical Quantum Confinement and Photocatalytic Properties in Two-, One- and Zerodimensional Nanostructures. *R. Soc. Open Sci.* **2018**, *5*, No. 180387.
(44) Van Dong, P.; Ha, C. H.; Binh, L. T.; Kasbohm, J. Chemical Synthesis and Antibacterial Activity of Novel-Shaped Silver Nanoparticles. *Int. Nano Lett.* **2012**, *2*, No. 9.
(45) Rashid, M. U.; Bhuiyan, K. H.; Quayum, M. E. Synthesis of Silver Nano Particles (Ag-NPs) and their Uses for Quantitative Analysis of Vitamin C Tablets. *Dhaka Univ. J. Pharm. Sci.* **2013**, *12*, 29−33.

https://doi.org/10.1021/acsomega.1c05374
ACS Omega 2022, 7, 4921−4931